FDTD Computer Modelling of a Half Wavelength (4π) Toroidal Cavity Mode With Spin and Angular Momentum

Michael Glen

19th October 2023

Abstract

The properties of a resonant half wavelength mode, sometimes called a 4π mode, is investigated in a toroidal cavity of large aspect ratio. No dividing wall is used but instead the field is given a poloidal (in the direction of the smaller circumference) twist. The toroidal cavity resonator equations are derived by bending a length of cylindrical waveguide into a toroid and changing the field equations from cylindrical to local toroidal. If the toroid aspect ratio is large the errors are small but the equations must still be considered to be approximate and so in order to confirm the stability and form of the resonant modes a finite difference time domain (FDTD) program was written to model the propagation of the fields. This also confirms that no false assumptions have been made, particularly regarding how the fields behave where the two ends of the half wave join. This is believed to be the first confirmation of the existence of a half wave toroidal mode without a dividing wall.

FDTD simulations of both a toroidal (in the direction of the larger circumference) and a poloidal spinning 4π mode were also carried out. It was observed that the presence of twist would prevent either a pure toroidal or poloidal spinning mode being produced and that the poloidally spinning field produced a stable mode with both spin and angular momentum.

1 Introduction

It might be thought that a half wave resonant mode in a toroidal cavity resonator without a dividing wall could not exist as consecutive half cycles would be of opposite phase and cause destructive interference, destroying any stable mode. However, it is shown in this paper that if the half wave field is progressively twisted about the poloidal angle by π as the toroidal angle increases from 0 to 2π then for some modes the second half wavelength has the same phase as the first and results in a stable field being produced. See Appendix A for details of toroidal cavity terminology and the local toroidal coordinate system used.

Cap and Deutsch, ref [1], found toroidal cavity fields using the scalar Helmholtz equation and noted that the equations had a 4π solution. This was investigated further by Deutsch in ref [2]. In later work, ref [3], Deutsch noted that many of the previously proposed solutions to the Helmholtz equation did not satisfy all the boundary conditions and Maxwell's equations. Finally just one 4π mode was found to be a valid solution and this needed a conductive radial separating wall completely blocking the toroid minor diameter cross section. It should be mentioned that Deutsch was working on the problem of finding the resonant modes of toroidal cavity resonators of any aspect ratio. This is difficult due to it not being possible to separate the variables of the wave equation when written in toroidal coordinates. The electromagnetic field configurations found vary depending on the aspect ratio and except

at large aspect ratios are not usually pure transverse electric (TE) or transverse magnetic (TM) modes.

For toroids with a large aspect ratio the above calculation difficulties do not apply and the field equations become much simpler as the fields are almost the same as in a cylindrical waveguide. These cylindrical solutions applied to a toroid have been called the cylinder or infinite aspect ratio approximation. The cylindrical waveguide solutions are well known and the field equations are shown in many textbooks, such as Balanis [4], and it is possible to express these equations in local toroidal coordinates as shown in Appendix B.

To provide confidence that the infinite aspect ratio field equations are valid for the toroidal modes being investigated and that a half wave mode is possible inside a toroidal cavity a finite difference time domain (FDTD) computer program was used to confirm the accuracy and stability of the field. FDTD programs are widely used to model how electromagnetic fields propagate. The difficulty with using them to model large aspect ratio toroidal cavities in this application is that in order to obtain just one half wavelength in the cavity the frequency used must be very near the cavity cut off frequency. In this condition a very small change in the toroid minor or major radius will cause significant changes in the field amplitude and wavelength and probably differences between radial and z axis polarisation results. It is not only individual cell smoothing (conformal modelling) which is necessary but both minor and major radii must be exactly circular to high accuracy to prevent such errors.

Initial attempts were made modelling the toroid using Cartesian coordinate FDTD programs but it was not found possible to eliminate these effects so an FDTD program was written in local toroidal coordinates. This used the exact equations (A.1) given in Appendix A for conversion from Cartesian to local toroidal coordinates so contained no approximations, unlike those to produce the initial fields in Appendix B. Maple 2016 was used and although this is probably not the best language for running fast FDTD code the new coordinates completely eliminated the spurious field variations. Increased computation speed would be desirable but all the results shown in this paper were obtained using just a desktop computer and a single processor core. In the FDTD simulations, for time step zero only, the toroid was filled with either just the E or H field or both fields together depending on the configuration it was required to test as a possible resonant mode. The simulation was then run to see how these initial fields developed. Non resonant modes show large transients or evolve into chaotic fields and only a resonant mode smoothly oscillates, periodically cycling back to its initial state. Originally the time zero fields were obtained using a short program written to produce toroidal field components directly from the cylindrical field equations using the cylinder approximation. More recently they have been obtained using the toroidal cavity field equations (B.33), in Appendix B.

To test the FDTD program it was necessary to have an initial field, the equations of which were valid at small aspect ratios. This brings into play terms in the local toroidal coordinate FDTD equations which are small at large aspect ratios but large at small aspect ratios. If these terms were incorrect they could invalidate the results even at large aspect ratios. Such fields are difficult to find in the literature so the Deutsch 4π field mentioned above was invaluable, even though it needed a dividing wall to be temporarily modelled in the program. A slight change was needed to the Deutsch equations to ensure the fields joined around the toroid but the mode was stable even at small aspect ratios and provided one of the best tests of the toroidal FDTD code.

2   A First Look at the TE_{11} Mode

The FDTD results being examined in this paper are restricted to just the TE_{11} mode and Appendix B describes how these mode numbers are derived. There are, of course many other modes which could be used but TE_{11} is the lowest frequency one which can exist in a toroid of a particular minor radius. The electric field distribution of this mode across the

toroid minor diameter is shown in Fig 1. This field can be rotated or spun poloidally so the field can point at any θ angle.
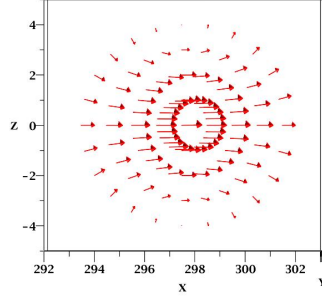
Figure 1: Minor Diameter Cross Section Showing TE_{11} Electric Field

In all the field plots in this paper only the length of the arrows shows the field strength. The density of the arrows is of no significance as it is just dependant on the the FDTD program field calculation positions used and selected for the plot. Unless otherwise stated all the FDTD simulations use a toroid with 8 grid squares across the minor diameter, 24 in the theta direction and 136 in the phi direction and an aspect ratio of approximately 74.427.

The TE_{110} magnetic field is shown in Fig 2 and for the magnetic field a third mode number of zero has been included. This defines the number of wavelengths around the toroid in the ϕ direction and zero means the field has no variation in this direction. As the figure shows the magnetic field for this particular mode has a simple form as only the H_ϕ field component is present.

An important point the two figures illustrate is the θ angle phase relationship between the electric and magnetic fields as the maximum and minimum field amplitudes are aligned. This occurs because a theta direction spinning electromagnetic field has been plotted which can be confirmed by checking the direction of the Poynting vector given by the $\vec{E} \times \vec{H}$ vector. For the E and H fields shown this results in anti-clockwise spin. Spinning fields are explained in more detail in ref [5] which examines spinning cylindrical and spherical cavity fields. For the more usual non-spinning field one of them would be rotated 90 degrees from its current position so that the maximum of one field lined up with the minimum of the other as discussed in the next section.
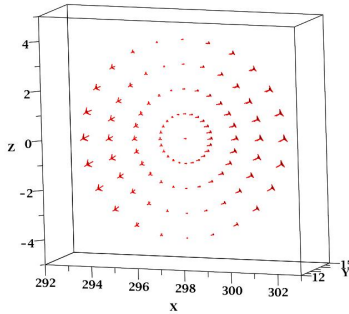
Figure 2: Minor Diameter Cross Section Showing TE_{110} Magnetic Field

3

3 FDTD Results For the Basic Non-Spinning Toroidal Twisted Half Wavelength $TE_{11\frac{1}{2}}$ Mode

To create this mode the simulation was started using just the electric field of a twisted half wave of the TE_{11} mode like that shown in Fig 3. References such as (C2=-1, F2=G2=1, T=-0.5) shown in this figure refer to the values needed in appendix equations (B.33) to produce the fields. Because the mode has one half wave in the phi direction the mode is designated as $TE_{11\frac{1}{2}}$. Initially there is no magnetic field but running the FDTD simulation shows the electric field gradually collapses to zero magnitude and as it does it produces a magnetic field similar to that in Fig 4. As the simulation continues the magnetic field collapses and produces an electric field which, by the time the magnetic field is zero, has the same magnitude as it did initially but is of opposite polarity, so is pointing in the opposite direction to that shown. This marks the completion of the first half cycle and after another half cycle the fields will have returned to their initial states. The 3D field plots shown were actually taken after the initial electric field had gone through 99,994 FDTD timesteps and the magnetic field 100021 timesteps which corresponded to approximately 925 cycles and demonstrates the stability of the mode and the accuracy of the simulation.
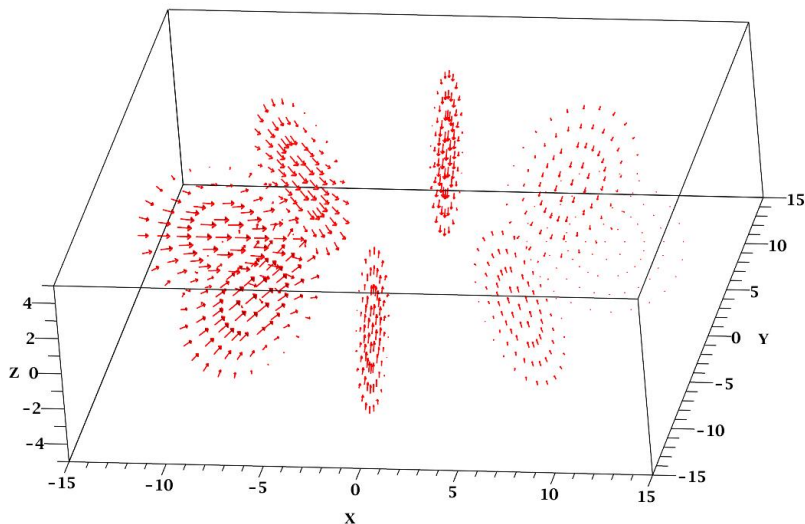
Figure 3: 3D Plot of $TE_{11\frac{1}{2}}$ Electric Field With a Toroid Aspect Ratio of Approx. 74.4. (C2=-1, F2=G2=1, T=-0.5)

In these 3D plots in order to try and display the field as clearly as possible just eight different ϕ angle locations, equally spaced around the toroid, have been chosen and the field there, across the minor diameter cross section, plotted. Although the toroid aspect ratio for this FDTD run was still approximately 74.427 if shown to scale the minor diameter, where the field is, would be too small to see any detail. To give a better view the 3D plot is displayed with the fields positioned as if the aspect ratio was 10. The plot shows the $\sin(\phi)$ amplitude of the field and the clockwise twist with increasing ϕ angle, when viewed in the direction of increasing ϕ angle (which is anti-clockwise when viewed from above). This convention of viewing in the direction of increasing ϕ angle will always be used when describing twist and spin rotations. The field 'join' is at $\phi = 0$ and either side of this the field is of opposite phase which is correct for when two half waves join. Viewed from outside the toroid the electric field lines are mainly pointing inward but as described above as the cycle continues the field will reverse and point outwards so the electric field is sinusoidally
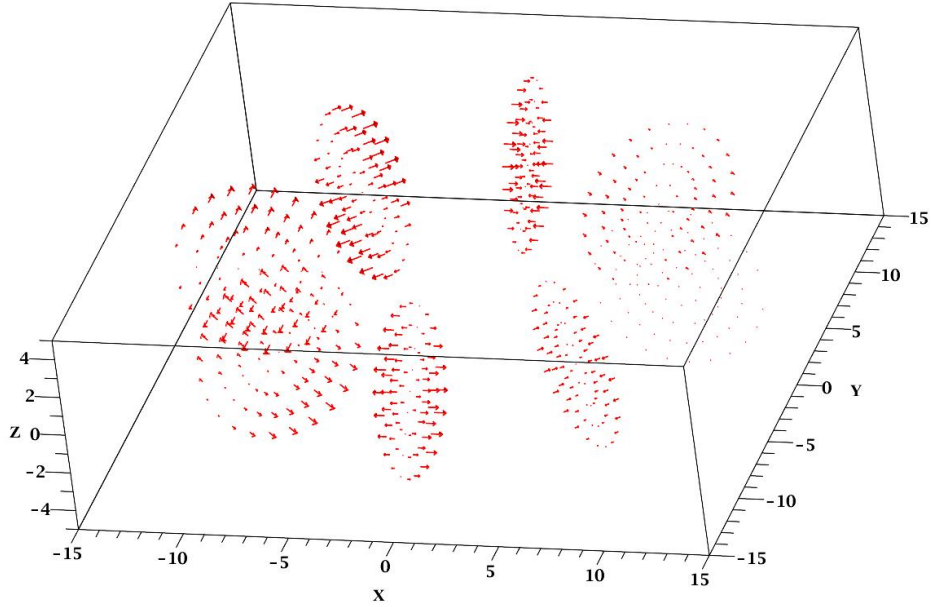
Figure 4: 3D Plot of $TE_{11\frac{1}{2}}$ Magnetic Field With a Toroid Aspect Ratio of Approx. 74.4

oscillating positive and negative. Because the fields only vary in magnitude and switch direction but do not rotate poloidally or toroidally they have no spin or orbital angular momentum which can be confirmed by checking the direction of the Poynting vector.

4 FDTD Results For a Toroidally Spinning Twisted Half Wavelength $TE_{11\frac{1}{2}}$ Mode

A toroidally spinning mode may be rotating in the positive or negative phi direction. Starting with electric and magnetic fields which are the same as those in Fig 3 and 4 for the stationary mode, they can be made to spin toroidally by rotating the starting magnetic field by 180 degrees (90 degrees electrical) in the $\pm\phi$ direction. In this case it has been $-\phi$ rotated and followed the theta twist to give the field shown in Fig 5. It may not be immediately obvious why this field combination produces a toroidally spinning field as the Poynting vector seems to have no resultant in the ϕ direction as the various components are equal and in opposite directions. However it is apparent that the magnetic field does not completely go to zero at the $\phi = 180$ degree position, where the electric field is a maximum. The magnetic field at this location is plotted in Fig 6 and as usual is shown viewed in the direction of increasing ϕ angle. In conjunction with the electric field this does give a Poynting vector in the $+\phi$ direction as required for anti-clockwise rotation when viewed from above in the 3D plots.

This anti-clockwise rotation is apparent in Fig 7 which has been plotted after 14 time steps which is just over $\frac{1}{8}$th of a cycle after the FDTD starting E field in Fig 3. In $\frac{1}{8}$th of a cycle a field might be expected to move $\frac{1}{8}$th of a revolution but has actually moved about $\frac{1}{4}$ of a revolution, so is twice the rotation rate normally expected. That is an excitation frequency of ω will give an apparent rotation rate of 2ω due to the field in the toroid being only half a wavelength and the field only having to travel half a wavelength instead of a full wavelength for a complete 360 degree phi rotation. It is for the same reason that after the first revolution of half a wavelength the field direction has reversed and has a sign of minus one and a further revolution is required for the field polarity to return to its initial state. This gives the half wave toroid field similar properties to a Mobius strip and two revolutions are required to return to the original state.

5
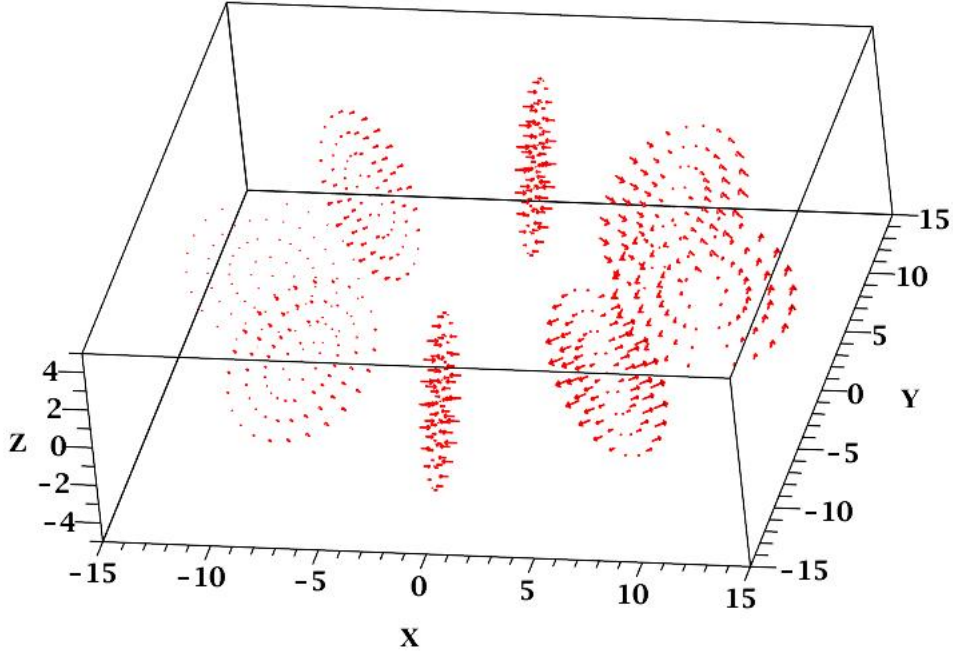
Figure 5: 3D Plot of $TE_{11\frac{1}{2}}$ Starting Magnetic Field Used to Produce Toroidal Spin (C2=-1, F2=G2=1, T=-0.5)
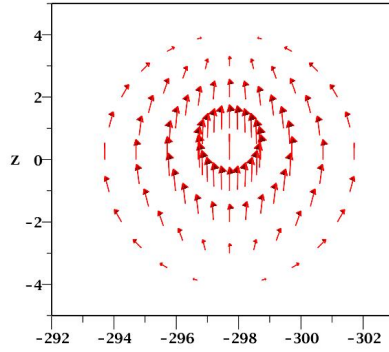
Figure 6: Plot at Phi Angle of 180 Degrees of $TE_{11\frac{1}{2}}$ Magnetic Field Across the Toroid Minor Diameter. (C2=-1, F2=G2=1, T=-0.5)

Further examination shows that the polarity of the electric field reverses 180 degrees as it passes through zero, so although the plot shows the electric field at the same theta angle at a particular ϕ position its amplitude is varying sinusoidally and its direction continually reversing. Next it will be shown that even these fields, which over a small timescale are at the same reversing theta angle, are actually slowly toroidally rotating at the group velocity.

The field toroidal rotation initially discussed was occurring at the phase velocity and this could be many times the velocity of light as toroids are being considered which have large aspect ratios and are operating very near their cut off frequency. The formula for finding the phase velocity in metres per second is:-

$$V_p = c\frac{\lambda_g}{\lambda_e} \tag{1}$$
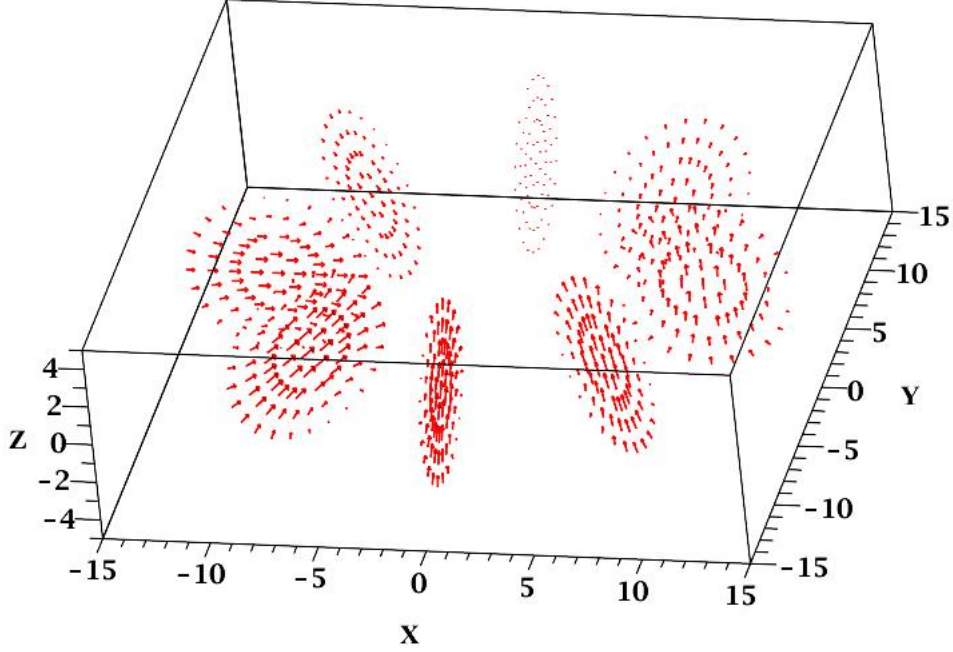
Figure 7: 3D Plot Of $TE_{11\frac{1}{2}}$ Electric Field After Approximately $\frac{1}{8}$th Of a Cycle.

Where:-
c is the velocity of light in metres per second.
λ_e is the wavelength of the toroid excitation frequency measured in air.
λ_g is the wavelength of the field in the toroid which for a half wavelength is $4\pi R$ with R being the toroid major radius. Near cut off frequency this will be many times λ_e.

The energy in the field is travelling at the group velocity which will be less than c and this is given, in metres per second, by the formula:-

$$V_g = \frac{c^2}{V_p} \tag{2}$$

The phi angle travelled (measured in degrees) in a given number of FDTD time steps ($N_{timesteps}$) due to this group velocity can then calculated using:-

$$\phi_{deg} = V_g \Delta t N_{timesteps} \frac{360}{2\pi R} \tag{3}$$

Where:-
Δt is the time represented by a single FDTD timestep in seconds.

It is actually possible to see this group velocity rotation if the FDTD simulation is run for a sufficient number of time steps. Fig 8 is plots of the radial, E_r (red), and theta direction, E_θ (turquoise), field strengths around the toroid in the ϕ direction at a position inside the toroid which is where $\theta = 0$ degrees and the minor toroid radius $r = 2$ FDTD grid squares (with the cavity wall at r = 4). Plot 8(a) is the initial starting electric field at time step zero and plot 8(b) is after 99,996 time steps, or approximately 925 cycles later. It is apparent that the two plots are similar but in the later plot the field distribution has moved slightly to the right, which is the plus phi direction.

7

(a) t=0   (b) t=99996
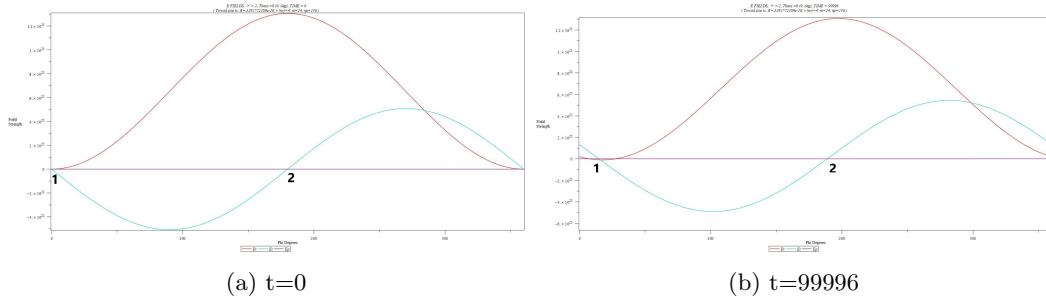
Figure 8: Amplitude Variation of E_r and E_θ Electric Field Components With ϕ Angle

A more accurate measurement of the amount of movement can be obtained by examining a field magnitude against phi angle plot similar to Fig 8 but which is basically produced with a much smaller phi angle range. To reduce errors the techniques shown in Appendix C were used which can include measurements of both the E_r and E_θ fields and select different theta angle measuring positions as well. This allows alternative measurements of the field toroidal travel to be compared to give confidence in the accuracy of the result. The phi angle travel distances found in Appendix C are summarised in Table 1 below. The calculated distances have been compared with that which would be expected if the field was travelling at the group velocity, calculated using eqn (3) as 8.89 phi degrees. The percentage error is shown in the last column of the table and these results confirm that within experimental limits the field is rotating at the theoretically calculated group velocity.

Table 1: Long Term Phi Direction Movement of Toroidally Spinning 4π Field
(Theoretical Group Velocity Movement 8.89 degrees)

Measuring Position				Result	
Field Component Used	Time Step Number	Approx. Phi Angle (degrees)	Theta Angle (degrees)	Phi Angle Travelled (degrees)	Error Compared With Theory (percent)
E_θ	99996	189	0 & 180	8.82	-0.79
E_r	99996	189	90 & 270	8.84	-0.56
E_θ	100021	9	90 & 270	8.97	+0.90
E_r	100021	9	0 & 180	8.97	+0.90

The reason the methods of Appendix C were adopted to measure the field movement is that although the field shows no sign of instability the exact form of the mode is changing slightly over time. The effects are too small to be visible in the 3D field plots but the increased sensitivity of the phi angle plots shows changes which have taken place to the initial starting field. The Appendix C techniques show there has been a small amount of poloidal movement which is apparent as it causes the phi angle at which a field component goes to zero to vary slightly over a half cycle. A method of choosing a time step which reduces the error due to this cause was used to more accurately measure the group velocity. The technique also clearly showed there was a very slight offset of the field from the centre of the minor diameter along the line of the major radius. Because of these field changes noticed in the plots it would be desirable to increase the number of FDTD time steps calculated in order to check if the form of the field continued to evolve. A run was carried out to a million time steps but it would also be necessary to reduce the time step length and increase the

8

number of grid squares used in the FDTD runs to check that any changes are not due to inaccuracies in the simulation and unfortunately the speed of the program used is not really sufficient to do this in a reasonable time at the moment.

5   FDTD Results For a Poloidally Spinning Twisted Half Wavelength $TE_{11\frac{1}{2}}$ Mode

The usual way to produce a poloidally spinning field in the laboratory would be to start with the $TE_{11\frac{1}{2}}$ electric field of Fig 3 and add to it a second electric field 90 degrees poloidally displaced from it, with its peak occurring a quarter of a cycle later in time. This is not possible using an FDTD simulation as all fields must be present at time step zero when the simulation starts and this second field would be zero then. Instead, still starting with the electric field of Fig 3, the second field is produced by including an initial magnetic field which is in phase with the initial electric field and as this decays it produces the required electric field displaced poloidally by ninety degrees and with the correct quarter cycle time delay. This initial magnetic field can be obtained by moving the whole of the twisted magnetic field poloidally by ninety degrees relative to the electric field, compared with its position in Fig 4. This will give the field shown in Fig 9.
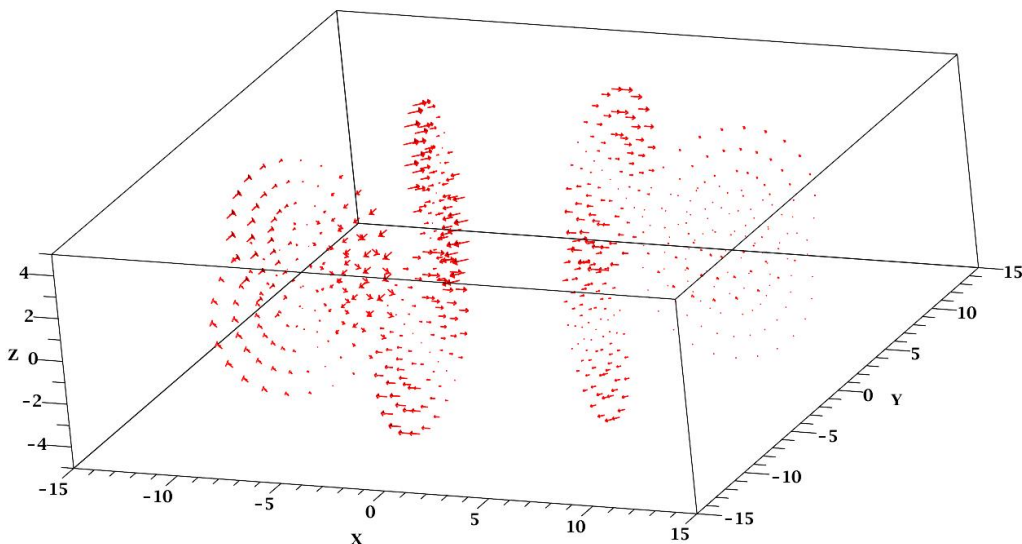
Figure 9: 3D Plot of $TE_{11\frac{1}{2}}$ Magnetic Field Required to Produce a Poloidally Spinning Field. (D2= E2=G2=1, T=-0.5)

As can be seen this completely aligns the maximums and minimums of the electric and magnetic fields i.e. they are in phase. At the surface of the toroid E_θ will be zero and as both E_r and H_ϕ have $\cos\theta$ and $\sin\phi$ amplitudes the E_r/H_ϕ amplitude ratio will be constant over the whole surface of the toroid. Calculating the direction of the Poynting vector from Figs 3 and 9 confirms it is anti-clockwise, which is the same direction as the observed field spin. The field is spinning poloidally at the toroid energising frequency, f_e. This results in cyclical reversal of the field with time so although at the instant plotted the electric field lines are predominantly pointing inward the field spin will make the field direction change to outward after half a cycle. The rotation is shown in Fig 10 which has been plotted 27 FDTD time steps after the initial E field, which is approximately $\frac{1}{4}$ cycle later.

Another significant difference between this and the toroidally spinning field in the previous section is that as this field spins it maintains a constant amplitude. It is the electric
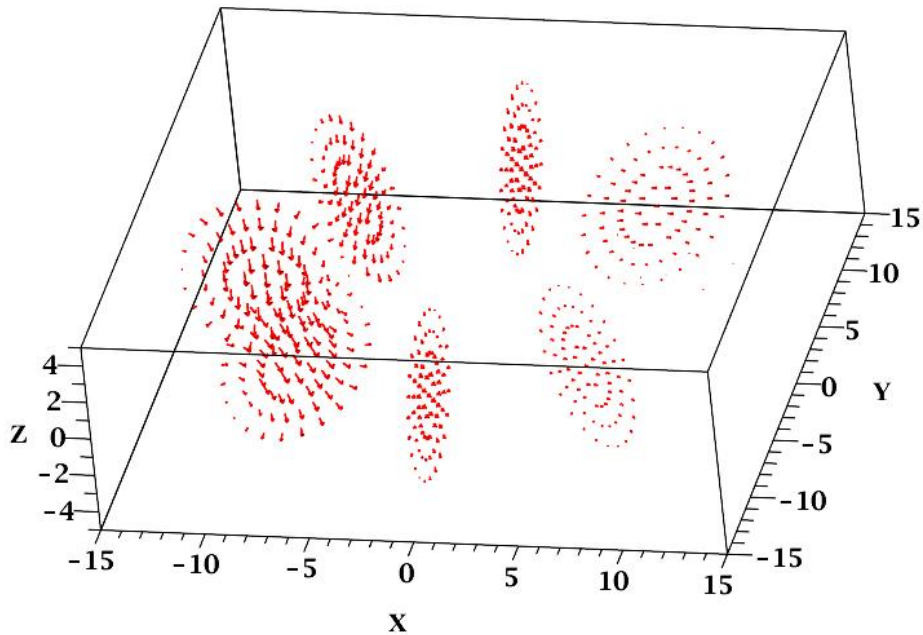
Figure 10: 3D Plot of $TE_{11\frac{1}{2}}$ Electric Field After Approximately $\frac{1}{4}$ Of a Cycle.

field changing position and not a change in amplitude of a stationary field with time which maintains the magnetic field and this magnetic field is also spinning and of constant amplitude. Both the E and H fields are twisted clockwise with increasing ϕ angle in this example. Reversal of the direction of spin can be done by moving the initial magnetic field poloidally by 180 degrees relative to the electric field. There is no relation between the direction of spin and twist so spin can be in the same or opposite direction to the twist.

As was done for the toroidally rotating field in section 4, plots of the field magnitudes from ϕ equals 0 to 360 degrees have been taken such as that for the electric field shown in Fig 11. This compares the field position at time step zero with the same fields after 99,994 time steps. Because of the poloidal spin the only reference points where the field magnitudes are zero over a short time period are at a phi angle of zero or 360 degrees. These can be used to assess field movement over longer timescales. The zero E_θ field point located near $\phi = 180$ degrees is an invalid reference as it moves from phi equals 0 to 360 degrees in just half a cycle. Comparing plots in Fig 11a and 11b it can be seen that there is a slight movement of the field by about 9 degrees in the phi direction but the amplitudes of both the field components are almost the same. The movement is small and there are no high frequency components or rapid field changes which would occur if this was an invalid mode.

To obtain a more accurate value for the movement a plot of E_θ and E_r can be done over a small phi angle range at the point where the field goes to zero, as in Fig 12 . This is similar to the plot technique used in section 4 but only the valid field zero reference point near $\phi = 9$ degrees must be used.

(a) t=0   (b) t=99994
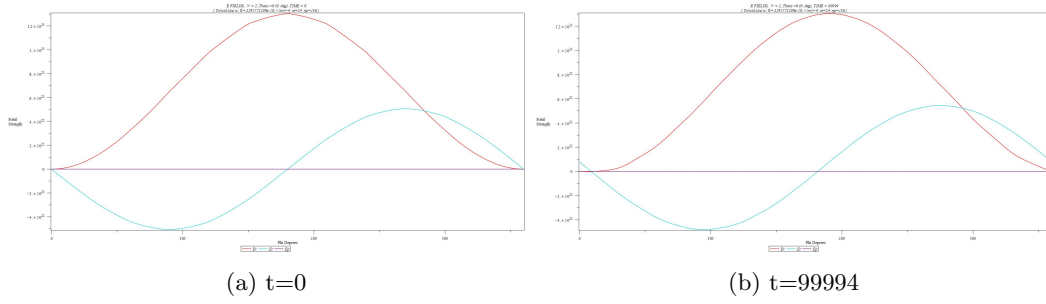
Figure 11: Amplitude Variation of E_r and E_θ Electric Field Components With ϕ Angle
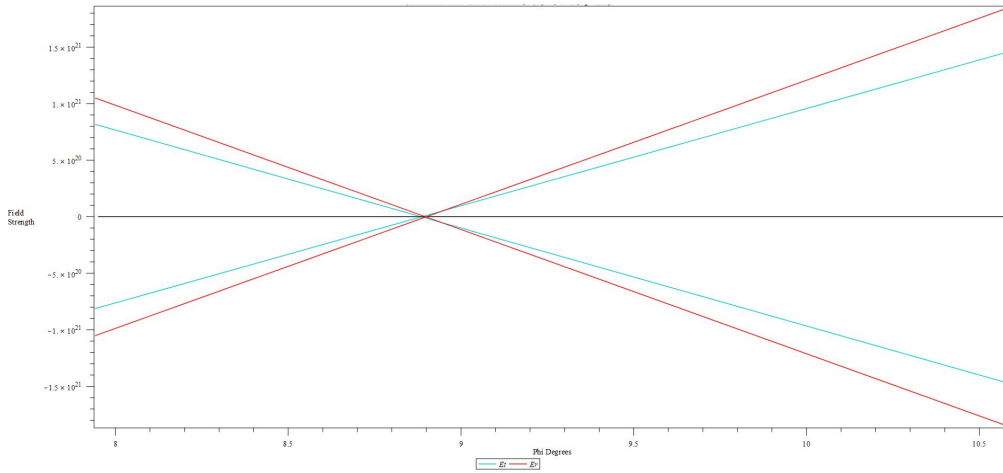
Figure 12: High Resolution Plot of E_θ and E_r Field Zero Magnitude Positions For t=99994.
(Turquoise E_θ Rising Line at $\theta = 180$ degrees, Falling Line at $\theta = 0$ degrees)
(Red E_r Rising Line at $\theta = 270$ degrees, Falling Line at $\theta = 90$ degrees)

The two E_θ field lines cross at zero field magnitude as do those for E_r. This shows that in this case, unlike for toroidal rotation, there is no offset of the field along the line of the major radius. There is also good agreement of the phi angle value of both the E_θ and E_r field zero points. Fig 12 gives a value for the phi direction movement of 8.90 degrees and this is similar to the movement previously obtained for the toroidally spinning field and the theoretical value of 8.89 degrees, confirming that this field is also moving at the group velocity.

It may be noticed that although this reading was taken at 99,994 time steps, other fields have been measured at 99,996 time steps. The reason for the difference is that these were the time steps selected using the measuring technique described in Appendix C. For the initial time step zero field it is zero magnitude everywhere across the whole of the minor diameter cross section for this measuring point, which would be positioned at phi=0 initially. For a small change in time step number therefore, the field zero would still be at phi=0. However, after almost 100,000 time steps very small changes have occurred to the field during the FDTD calculation. These cause the zero field position to oscillate over a cycle and this has some affect on the result. The alteration it makes to the value of the phi angle obtained is slight and it was checked that for this field the phi angle changed by only about 0.02 degrees per time step, i.e. a phi angle measurement of 8.86 degrees at time step 99,996.

More concerning is that for the poloidally spinning field the reason for any toroidal movement is not immediately apparent. It has already been confirmed that the Poynting vector for the main field visible in the 3D field plots points in the poloidal direction. If the

11

field is examined at the $\phi = 0$ position the E field is zero there and a plot of the magnetic field is shown in Fig 13. The magnetic field either side of this position has a similar form apart from the addition of a H_ϕ component, but this component could only result in poloidal rotation, not toroidal.
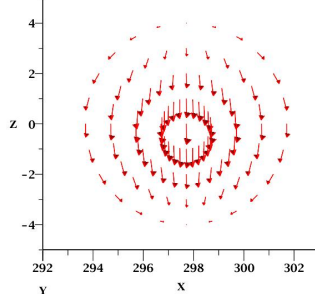
Figure 13: Magnetic Field Across Minor Diameter at $\phi = 0$ Degrees.

The electric field is examined either side of the $\phi = 0$ degrees zero field position in Fig 14. Looked at in conjunction with the Fig 13 magnetic field this does give rise to Poynting vectors in both the $\pm\phi$ directions but these are in opposite directions in alternate quadrants at a particular ϕ angle and also in opposite quadrants for ϕ angles either side of zero. This means all the ϕ direction Poynting vector components cancel out and so can cause no toroidal rotation. There is another possible source of toroidal movement and this is the twist which was introduced to enable either side of the half wave fields to join and this is investigated in the next section.

(a) $\phi = 2.65$ degrees

(b) $\phi = 357.35$ degrees
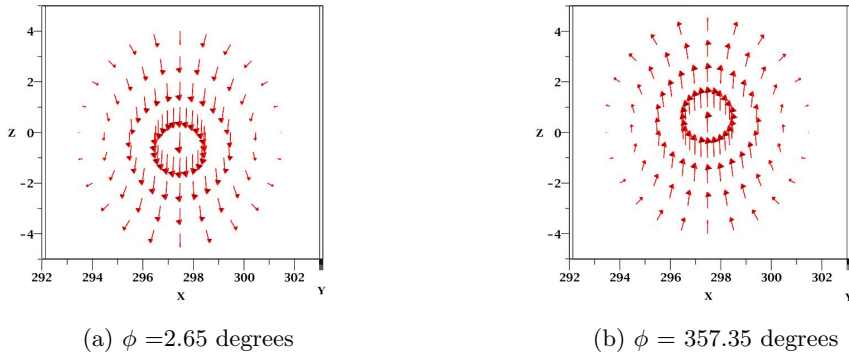
Figure 14: Electric Field Across Minor Diameter Either Side of $\phi = 0$ Degrees Position.

6   Investigation of the Effect of Twist

It is well known that a circularly polarised light beam has spin and hence spin momentum. Similarly introducing a twist to the light from a laser beam such that it has, in r, θ, z cylindrical coordinates, an $e^{il\theta}$ amplitude distribution, where l is an integer defining the amount of twist, is found to give it additional angular momentum. As rotational momentum is defined by a vector along the axis of rotation this vector will be in the z direction and is called optical or alternatively orbital angular momentum (OAM). See for example Allen et al ref [6] or for more papers the book Optical Angular Momentum ref [7]. The amplitude of

this OAM is proportional to l and to the energy in the beam and if the energy is considered to be in photons then the angular momentum can be calculated to be $l\hbar$ per photon. It has to be acknowledged that the twisted light beam has helical wavefronts and a zero intensity field along its central axis so has a different form from the field in the toroidal cavity. but it does show that twist can introduce additional momentum to a field.

In a toroid and using toroidal coordinates this would correspond to a beam travelling in the ϕ direction being given a twist l, called T using our nomenclature, in the θ direction. This should then cause angular momentum in the θ direction and hence an additional ϕ direction OAM vector. That situation is represented by a toroidally spinning field such as that in section 4 but the identification of what part of the momentum is spin and what is angular momentum being used there is not the same. In a toroid it seems natural to use the centre of the toroid, where $R = 0$, as the reference position and in that case poloidal rotation is spin and toroidal rotation is angular momentum. It was found that toroidal rotation did give rise to poloidal spin after a sufficient number of time steps. This was visible after a million time steps and the reason for requiring a high number is most likely because the large toroid aspect ratio results in a group velocity of less than 0.05% c and the very small amount of poloidal rotation this produces needs many time steps before it is sufficient to be detected in that FDTD simulation.

The situation with the poloidally spinning field discussed in section 5 although somewhat similar is different as the electromagnetic wave can initially be considered to be only travelling in the θ direction and this is a highly rotational, not linear, movement. The group velocity of this motion varies with r but is near the velocity of light. Despite the obvious differences compared with the laser beam OAM example it is possible that in this case also twist is responsible for the ϕ direction motion found to occur with the the poloidally spinning toroidal field. To test this, FDTD simulations were carried out using a TE_{111} mode which has one complete wavelength around the toroid instead of just a half wavelength. The advantage of this is that a stable full wavelength mode can exist without requiring any twist at all and so any ϕ direction movement in this zero twist case can be compared with the same field having ± 1 twist.

The toroid major radius and aspect ratio were initially kept the same as for all previous plots and the results of the tests are shown in Table 2. The time step at which to measure the group velocity ϕ angle was found using the method described in Appendix C. For the test with no twist the movement was only 0.01 degrees whereas for +1 twist it was +17.51 degrees and for -1 twist -17.50 degrees. This confirms that the toroidal direction movement is indeed due to the presence of twist. Looking at the results from Tables 2 and 3 it is apparent that movement is in the plus phi direction if theta twist and spin are in opposite directions and in the minus phi direction if they are in the same direction.

Table 2: Phi Direction Movement of Poloidally Spinning One Wavelength Field (Radius of 1R)

Twist (T)	Theta Twist (degrees)	Theta Spin Direction	Measure At Timestep	Phi Direction Movement (degrees)
0	0	clockwise	99993	+0.01
+1	360 anti-clockwise	clockwise	99995	+17.51
−1	360 clockwise	clockwise	99995	−17.50

Equations are given in this paper for the magnitude of the group velocity and the number of degrees of phi direction movement this produces for a toroidally spinning field. It is now possible to check if the experimental results for the group velocity movement of the twisted poloidally spinning field give the same result. Using eqn (3) for the phi direction movement in degrees and substituting for V_g using eqn (B.27) in Appendix B, remembering that $V_g = cv_g$,

Table 3: As Table 2 But Major Radius Increased From R to 2R

Twist (T)	Theta Twist (degrees)	Theta Spin Direction	Measure At Timestep	Phi Direction Movement (degrees)
+1	360 anti-clockwise	clockwise	99982	+4.42
+1	360 anti-clockwise	anti-clockwise	99982	−4.42

results in the relationship:-

$$\phi_{deg} = \frac{180c^2}{\pi} \frac{pt}{\omega_e R^2} \tag{4}$$

Where t is now the FDTD simulation time in seconds which has replaced $\Delta t N_{timesteps}$ in eqn (3).

As all the phi distance measurements were carried out at the same value of t to within 2 parts in 10,000 and the same excitation frequency ω_e was also used, eqn (4) becomes:-

$$\phi_{deg} \propto \frac{p}{R^2} \tag{5}$$

The phi angle movement for the poloidally spinning half wave field was found to be 8.90 degrees in Fig 12. The Table 2 fields have the same value of R but double the wavelength and hence double the p value so eqn (5) predicts twice the phi direction movement which is 17.80 degrees. Table 3 also has twice the p value but twice R value too so the calculated phi movement is just $\frac{17.8}{2^2}$ or 4.45 degrees. The measured values in Tables 2 and 3 are all within 1.7% of these predicted values and, within the limits of the experiments, the group velocity movement is the same for the twisted poloidal spinning fields as for toroidal spinning ones.

The twist for these simulations was one complete phi direction twist per wavelength, hence for a half wavelength field just half a twist. A test was also carried out using a 9R radius toroid containing 5 half waves, firstly with one twist per wavelength (2.5 twists) and then with just $\frac{1}{5}$ twist per wavelength (0.5 twists). The 2.5 twist field travelled 5 times the phi distance compared with the 0.5 one. Although this was only a single comparison it indicates the phi distance travelled by poloidally spinning fields is actually proportional to the twists per wavelength ($\frac{T}{p}$).

7 Conclusion

The FDTD computer simulations which are reported here have confirmed the existence of the half wave toroidal modes and that they do not go unstable, although they can change the detailed form of their mode. The poloidally spinning mode is the most stable though. Further tests are desirable to investigate long term stability but a faster FDTD simulation would be necessary to do this.

David Hestenes has published a number of papers, such as ref [8] and [9] analysing the Dirac equation and the sort of physical system the mathematics is describing. He favours a model having a point electron on a lightlike toroidal vortex but in the first reference also comments that the Dirac equation could be describing a similar distributed electron. The poloidally spinning field in this paper appears to be a good fit for a Hestenes distributed model which, due to its twist, has both spin and angular momentum. Poloidal spin results in a mode with a constant E_r to H_ϕ field magnitude ratio which only varies with frequency and this gives it the potential to satisfy its own boundary conditions. The conversion of the oscillating polarity toroidal charge to either positive or negative is an interesting problem but if time permits it is hoped to publish a further paper looking at the properties of such a self trapped toroidal cavity electron.

APPENDIX A

A   - Toroidal Coordinates and Toroid Nomenclature.

Only local toroidal coordinates are used in this paper. These are also sometimes called simple toroidal coordinates, quasi toroidal coordinates, normal toroidal coordinates or poloidal coordinates but all are the same. They are based on cylindrical coordinates as the outer tube of the toroid can be treated as a bent cylinder. The distance measured from the centre of the toroid to the centre of the outer cylinder is known as the major radius (R) as shown in Figure A.1. The radius of the cylinder (r_0) is the minor radius and the ratio R/r_0 is called the aspect ratio. The inverse of this (r_0/R) is the inverse aspect ratio. For a large aspect ratio the bent toroidal cylinder could be considered to be almost straight and the results obtained by treating the toroid as a cylinder are known as the cylinder or infinite aspect ratio approximation.
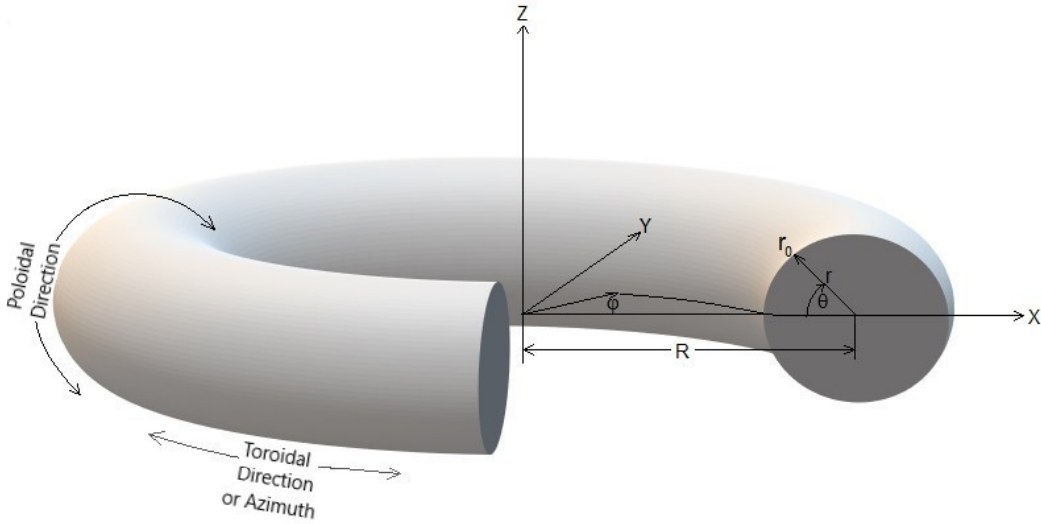
Figure A.1: Diagram of Toroid Including Local Toroidal Coordinates

Note that the convention adopted here is the same as in Cap and Deutsch [1] and the θ angle is zero when r points towards the centre of the toroid and increases in a clockwise direction when looking along the cylinder in the direction of increasing ϕ. When referring to directions, motion following the larger toroid circular ring, which involves changes in only the ϕ angle, is commonly known as toroidal or azimuthal. Motion following the smaller toroid circumference, which changes just the θ angle, is poloidal.

The above figure also shows the Cartesian coordinate axes with the origin at the centre of the toroid. It is often needed to translate between toroidal and Cartesian coordinates and the equations to do this are:-

$$x = (R - r\,cos(\theta))\,cos(\phi) \tag{A.1a}$$
$$y = (R - r\,cos(\theta))\,sin(\phi) \tag{A.1b}$$
$$z = r\,sin(\theta) \tag{A.1c}$$

APPENDIX B

B - Field Equations For a Toroidal Cavity Resonator in Local Toroidal Coordinates Using the Cylinder Approximation

B.1   Conversion of Equation Coordinates From Cylindrical to Local Toroidal.

The cylindrical coordinate system is well known and the axes are usually labelled r, θ and z or alternatively ρ, ϕ and z. If the cylinder is bent to form a toroid these become r, θ and ϕ respectively, as shown in Appendix A. The toroid major radius, R, also needs to be specified and the relationship between the cylindrical and local toroidal coordinates using the cylinder approximation is then:-

$$\textbf{Cylindrical to Toroidal} \tag{B.1}$$

$$r \text{ OR } \rho \;=\; r$$
$$\theta \text{ OR } \phi \;=\; \theta$$
$$z \text{ OR } z \;\approx\; R\,\phi$$

An equation written in cylindrical coordinates can be changed to local toroidal coordinates by making the above substitutions. This is only approximately valid as more accurately $z = (R - r\cos(\theta))\,\phi$ which is why these toroidal equations only apply to large aspect ratio toroids where $R \gg r$ and the $r\cos(\theta)$ term becomes negligible. The resulting approximate equation is still applicable when using the the coordinate convention shown in Appendix A where θ is measured from what would be the -x cylindrical axis and increases in a clockwise direction rather than using the cylindrical coordinate convention where θ would be zero along the +x axis and increase in the anti-clockwise direction. Both are right handed coordinate systems.

B.2   Initial TE Field Equations For a Large Aspect Ratio Toroidal Cavity

The field equations for a cylindrical waveguide can be found in many text books and one such source, which, like this paper, uses SI units is Balanis [4]. Another much earlier book is H.R.L. Lamont [10] which uses cgs units so the equations are slightly different and for our identical mnp Balanis mode parameters it uses nmν so comparison can be confusing. Nevertheless its concise yet thorough treatment of waveguide and cavity modes makes it a very helpful reference. In this paper only TE fields are being considered, not TM, and making the above substitutions in the Balanis equations gives the initial toroidal cavity field equations in local toroidal coordinates for the TE_{mn} modes. The equations will be developed further when the field boundary conditions and the use of field twist and spin are taken into account later in this appendix:-

$$Er = -A_{mn}\,\frac{m}{e_0\,r}\,\left(J_m\,(k\,r)\right)\left[-C_2\sin(m\theta) + D_2\cos(m\theta)\right]e^{-j\beta R\phi}\;e^{+j\omega t} \tag{B.2a}$$

$$E_\theta = +A_{mn}\,\frac{k}{e_0}\,\left(-J_{m+1}\,(k\,r) + \frac{mJ_m\,(k\,r)}{k\,r}\right)\left[C_2\cos(m\theta) + D_2\sin(m\theta)\right]e^{-j\beta R\phi}\;e^{+j\omega t} \tag{B.2b}$$

$$E_\phi = 0 \tag{B.2c}$$

$$Hr = -Amn\,\frac{k\beta}{\omega\,\mu_0\,e_0}\,\left(-J_{m+1}\,(k\,r) + \frac{mJ_m\,(k\,r)}{k\,r}\right)\left[C_2\cos(m\theta) + D_2\sin(m\theta)\right]e^{-j\beta R\phi}\;e^{+j\omega t} \tag{B.2d}$$

$$H_\theta = -A_{mn}\,\frac{m\beta}{\omega\,\mu_0\,e_0\,r}\,\left(J_m\,(k\,r)\right)\left[-C_2\sin(m\theta) + D_2\cos(m\theta)\right]e^{-j\beta R\phi}\;e^{+j\omega t} \tag{B.2e}$$

$$H_\phi = -Amn\,\frac{k^2}{\omega\,\mu_0\,e_0}\,\left(J_m\,(k\,r)\right)\left[C_2\cos(m\theta) + D_2\sin(m\theta)\right]je^{-j\beta R\phi}\;e^{+j\omega t} \tag{B.2f}$$

Note:

1) Compared with Balanis the following changes have been made in the above equations:-

1.1) Expressions involving partial differentials of Bessel functions have been replaced with equivalent ones containing none differentiated Bessel functions using the relationship:-

$$J'_m\,(k\,r) = \frac{\partial\left(J_m\,(k\,r)\right)}{\partial\,(k\,r)} = \left(-J_{m+1}\,(k\,r) + \frac{mJ_m\,(k\,r)}{k\,r}\right) \tag{B.3}$$

1.2) In addition to the ρ, ϕ and z coordinate substitutions some of the other symbols used in the Balanis equations have been changed:-

a) β_z is now β.

b) β is now k.

c) ϵ_0 and μ_0 are used instead of ϵ and μ as the relative permittivity and permeability are assumed to be equal to one. This is only strictly correct for a toroid containing a vacuum but the difference with air is extremely small.

d) $e^{-j\beta_z z}$ has been replaced by $e^{-j\beta R\phi}$. This uses the β_z substitution, item **a)** above, and replaces the Balanis distance along the cylinder (z) by the corresponding distance around the toroid, $R\phi$.

e) An $e^{+j\omega t}$ term is explicitly shown for each field component to denote how it changes with time. This term is omitted in most texts but its presence is always assumed.

2) Further explanation of equations:-

2.1) A_{mn} is just a constant which can be set to give the desired amplitude of the field. Defining it using the mn mode parameters allows different amplitudes to be selected for each mode.

2.2) Usually either θ phase selection constant C_2 or D_2 is put equal to one and the other constant put equal to zero. $D_2 = 1$ rotates the field 90 degrees plus theta, which is clockwise relative to $C_2 = 1$. If a value were given to both constants the field could be positioned at any desired θ angle. This will also usually alter the field component amplitude but if necessary this could be corrected by dividing each field component by $\sqrt{(C_2)^2 + (D_2)^2}$

2.3) The $e^{-j\beta R\phi}$ and $je^{-j\beta R\phi}$ terms could be replaced by sine and cosine terms using the trig expansion:-

$$e^{-j\beta R\phi} = \cos\left(\beta R\phi\right) - j\sin\left(\beta R\phi\right) \tag{B.4}$$

$$je^{-j\beta R\phi} = j\cos\left(\beta R\phi\right) + \sin\left(\beta R\phi\right) \tag{B.5}$$

Taking the real part of this expression would give a $\cos\left(\beta R\phi\right)$ replacement term for E_r, E_θ, H_r and H_θ but due to the presence of the j term in the equation for H_ϕ this would select a $\sin\left(\beta R\phi\right)$ term for this field component. Alternative replacement terms could be obtained by first multiplying all field components by j in which case the terms would be $\sin\left(\beta R\phi\right)$ for E_r, E_θ, H_r and H_θ and $-\cos\left(\beta R\phi\right)$ for H_ϕ.

To summarise, if additional new phase selection constants E_2 and F_2 are added to select the possible terms then alternative replacement expressions for $e^{-j\beta R\phi}$ (and $je^{-j\beta R\phi}$ for H_ϕ) are:-

$$\text{For } E_r,\ E_\theta,\ H_r \text{ and } H_\theta = E2\cos\left(\beta R\phi\right) + F2\sin\left(\beta R\phi\right) \tag{B.6}$$

$$\text{For } H_\phi = E2\sin\left(\beta R\phi\right) - F2\cos\left(\beta R\phi\right) \tag{B.7}$$

2.4) For a waveguide operating above its cut off frequency the field will travel along it. This can be more easily seen in the equations by combining the the waveguide $\beta R\phi$ distance exponential term with that for time to give:-

$$e^{-j\beta R\phi}\ e^{+j\omega t} = e^{-j(\beta R\phi - \omega t)} \tag{B.8}$$

A position on the wave of constant magnitude will require to satisfy the condition that:-

$$\beta R\phi - \omega t = \text{Constant} \tag{B.9}$$

Differentiating this expression with respect to t gives:-

$$\frac{\beta R\phi}{dt} - \omega = 0 \tag{B.10}$$

$\frac{R\phi}{dt}$ is an expression of distance over time so is the velocity of points of constant magnitude or phase. This phase velocity, V_p, in metres per second is therefore:-

$$V_p = \frac{\omega}{\beta} \tag{B.11}$$

Frequently the phase velocity is expressed as a multiple of the velocity of light instead, in which case it has no units and is just a numeric value the expression for which is:-

$$v_p = \frac{\omega}{\beta c} \tag{B.12}$$

Before the equations (B.2) can be used to plot the field it is necessary to know the values of all the parameters in them. The field boundary conditions at the cylinder wall determine m, n and k and this is the case for a cylindrical waveguide, cylindrical cavity or toroid. The process is well known and described in many text books but for completeness a brief summary is given in the next section.

B.3 Field Boundary Conditions at the Cylindrical Waveguide or Toroid Wall

The exact form of the field is determined by the boundary conditions it must satisfy and these are that at a conducting wall the electric field must be normal (ie perpendicular) to it or zero and the magnetic field must be parallel to it or zero. These conditions will be the same for both the cylindrical waveguide and the toroid wall. Considering the E field components E_r is perpendicular to the wall and the field equations have $E_z, (E_\phi$ for the toroid), set to zero so these two field components always satisfy the boundary condition.

For E_θ to be zero at the circular cylinder or toroid wall, from the field equation (B.2b) it can be seen that the differentiated Bessel function $J'_m(k\,r)$ must be zero when r equals r_0. Plots of two differentiated Bessel functions are shown in Figure B.1 and for m equal to one the first zero of the Bessel function occurs at approximately kr equal to 1.8. A more accurate value can be found in tables of differentiated Bessel function zeros such as given in Balanis and is more precisely equal to 1.8412. This first zero is said to be when n equals one so the equation to determine the value of k needed to satisfy the boundary condition at the cylinder wall for a TE_{11} mode is:-

$$k = \frac{1.8412}{r_0} \tag{B.13}$$
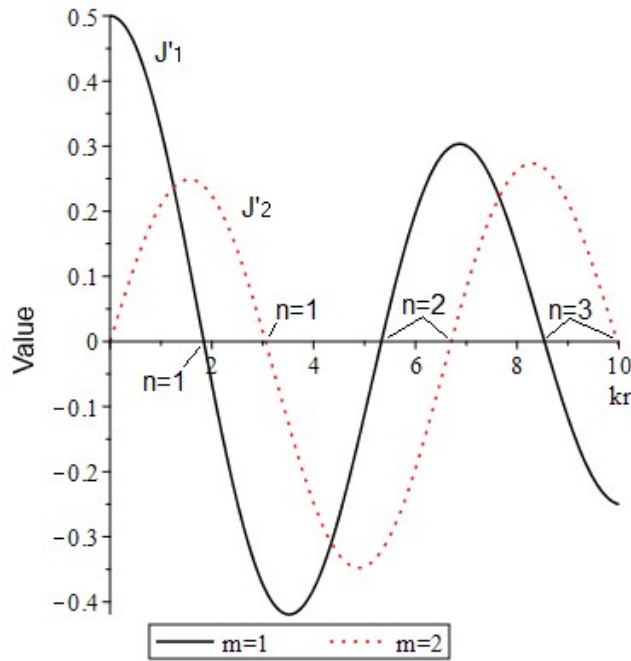
Figure B.1: Plot of Bessel Functions J'_m (for m=1 and m=2)

Again looking at the plot the second zero (when n equals two) of $J'_1(k\,r)$ occurs at kr equal to about 5.3 or more accurately 5.3315 so for the TE_{12} mode the boundary conditions are satisfied when $k\,r_0 = 5.3315$.

Considering the H field equations (B.2d to B.2f), H_θ and $H_z (H_\phi)$ are parallel to the curved cylinder (toroid) wall so always satisfy the boundary conditions. H_r contains a $J'_1(k\,r)$ term so the E_θ boundary condition, which requires the differentiated Bessel function to be zero when r is equal to r_0, will also make H_r zero. Having found the values of m and n this is sufficient to meet all the field boundary conditions at the circular cylinder/toroid wall and to determine the modes. If the waveguide/toroid energising frequency is too low no mode will be able to travel along it and the the frequency at which this occurs is known as the cutoff frequency. There are some common formulae derived in waveguide/cavity textbooks which are very useful and one of these enables the cut off frequency f_{co} to be found:-

$$f_{co} = \frac{c\,k}{2\pi} \tag{B.14}$$

As $\lambda = c/f$ this corresponds to a wavelength at cut off frequency (λ_{co}) of:-

$$\lambda_{co} = \frac{2\pi}{k} \tag{B.15}$$

Another textbook formula is for β:-

$$\beta = \sqrt{\frac{\omega_e^2}{c^2} - k^2} \tag{B.16}$$

Where ω_e is at the excitation angular frequency. There are two further wavelengths it is useful to know, λ_g, the wavelength in the cylinder or toroid and λ_e, the excitation frequency wavelength in free space (not in the waveguide):-

$$\lambda_g = \frac{2\pi}{\beta} \qquad \lambda_e = \frac{c}{f_e} \tag{B.17}$$

Substituting the three expressions for the various wavelengths in the equation for β gives the relationship between the three of them, which is:-

$$\left(\frac{1}{\lambda_g}\right)^2 = \left(\frac{1}{\lambda_e}\right)^2 - \left(\frac{1}{\lambda_{co}}\right)^2 \tag{B.18}$$

This equation shows that if the excitation wavelength is only slightly shorter than the cutoff frequency wavelength, so $1/\lambda_e$ is only slightly greater than $1/\lambda_{co}$, then $1/\lambda_g$ will be very small and the wavelength in the cylinder (λ_g) becomes very long. This is the condition in which a large aspect ratio toroid containing one, or just a half, wavelength will be operating.

B.4   Toroidal Cavities

Although the boundary conditions for toroidal cavities are mostly the same as those of a cylindrical cavity they are different at the position of the end wall. For a toroid where the wall is absent it is only necessary that the field is not cancelled by destructive interference at this location, a requirement which is most easily satisfied by having a whole number of wavelengths around the circumference of the toroid. This will also ensure that each field component is identical at zero and 360 degrees and there will be no field discontinuity where the wave "joins". Looking at eqns (B.6) and (B.7) in note 2.3 for the (B.2) toroidal field equations, it is apparent that all the field components present have a $\sin(\beta R\phi)$ or $\cos(\beta R\phi)$ amplitude in the ϕ direction. If p is the number of wavelengths around the toroid then each wavelength occupies a ϕ angle in radians of:-

$$\phi = \frac{2\pi}{p} \tag{B.19}$$

The sine and cosine terms must repeat after this angle so it is necessary that when ϕ has this value the argument of these trig functions is 2π. That is:-

$$\beta R\phi = \beta R \left(\frac{2\pi}{p}\right) = 2\pi \tag{B.20}$$

Therefore:-

$$\beta = \left(\frac{p}{R}\right) \qquad\qquad p = 0, 1, 2, 3 \ldots \tag{B.21}$$

The p=0 option makes $\beta = 0$ and therefore $e^{-j\beta R\phi} = 1$. All the field components present (E_r, E_θ and H_ϕ) have a constant amplitude in the toroidal (ϕ) direction and this is a toroidal TE_{110} mode. The mode is not possible in a cylindrical cavity because the fields cannot satisfy the boundary conditions at the cavity end wall.

After substituting p/R for β, the $e^{-j\beta R\phi}$ terms in field equation (B.2) become:-

$$e^{-j\beta R\phi} = \cos(p\phi) - j\sin(p\phi) \tag{B.22}$$

or, using phase selection constants as in note 2.3 of eqns (B.2):-

$$e^{-j\beta R\phi} = E2\cos(p\phi) + F2\sin(p\phi) \tag{B.23}$$

To find the resonant frequency formula for the toroid, starting with eqn (B.16) for β, replace ω_e by $2\pi f_e$ and substitute for β using eqn (B.21). Then re-arrange the resulting equation to obtain:-

$$f_e = \frac{c}{2\pi}\sqrt{\left(\frac{p}{R}\right)^2 + k^2} \tag{B.24}$$

For a wave travelling in the ϕ direction the equation for β in eqn (B.21) also enables it to be shown that the ratio of the wavelength in the toroid λ_g to that in free space λ_e is equal to the phase velocity. It is just necessary to use the wavelength equations (B.17) and substitute $\omega_e/(2\pi)$ for f_e. The final terms are then the same as in the phase velocity equation (B.12):-

$$\frac{\lambda_g}{\lambda_e} = \frac{2\pi}{\beta}\frac{\omega_e}{2\pi c} = \frac{\omega_e}{c\beta} = v_p \tag{B.25}$$

A useful relationship can be obtained from eqn (B.25) by substituting v_g for v_p using:-

$$v_g = 1/v_p = \frac{c\beta}{\omega_e} \tag{B.26}$$

and then substituting $\frac{p}{R}$ for β:-

$$v_g = \frac{cp}{\omega_e R} \tag{B.27}$$

B.4.1 Half-wave Toroidal Cavities

With the field configurations which have been looked at so far a half wavelength resonant mode could not occur as the fields include $\cos(p\phi)$ terms, or more precisely they will be $\cos\left(\frac{\phi}{2}\right)$ terms for a half wavelength. Such a cosine field will not join at ϕ equals zero and 360 degrees because one side will be positive and the other negative but if the field is twisted 180 degrees in the θ direction between ϕ equals zero and 360 degrees there is the possibility it will join. The most obvious way to do this might seem to be by creating a circularly polarised field. However, this no longer has a $\cos\left(\frac{\phi}{2}\right)$ waveform but is of constant magnitude at all ϕ positions and a circularly polarised half wave twist makes the field point in the opposite theta direction after half a wavelength so this will not join either. The other way is to just twist the original fields in the θ direction and this can be done by changing the θ terms in eqn (B.2) as follows:-

$$\sin(m\theta) \quad \text{becomes} \quad \sin(m\theta + T\phi) \tag{B.28}$$

$$\cos(m\theta) \quad \text{becomes} \quad \cos(m\theta + T\phi) \tag{B.29}$$

The minimum necessary twist of 180 degrees between ϕ equals 0 and 360 degrees is obtained with a twist parameter (T) of one half. Greater twists of 540, 900, 1260... degrees are also valid and so the complete possible range of values is:-

$$T = \pm\frac{1}{2}, \pm\frac{3}{2}, \pm\frac{5}{2}, \pm\frac{7}{2} \ldots \tag{B.30}$$

The $\pm$ sign allows twist in the negative or positive θ direction.

For completeness it is worthwhile noting that a multiple of 2π radians of twist could be used with one of the full wavelength modes. In this case permitted values of T would be:-

$$T = 0, \pm 1, \pm 2, \pm 3 \ldots \tag{B.31}$$

Having half wave resonant modes and if required 3/2, 5/2 etc wavelength modes around the toroid allows p to have not only the positive integer values previously given for the whole wavelength modes but now also half integer values of:-

$$p = \frac{1}{2}, \frac{3}{2}, \frac{5}{2} \ldots \tag{B.32}$$

It is necessary to confirm that this twisted field does join and still satisfies Maxwell's equations and this has been done using an FDTD computer simulation of the field within a toroidal cavity resonator. The exception to this is for the p=0 toroidal mode which is valid for integer twists but not for half integer ones which prevent the field joining.

B.4.2 Toroidal Cavity Field Equations

The set of equations (B.2) can now be modified by using the expansion given in note 2.3 of those equations on both the $e^{-j\beta R\phi}$ and $e^{+j\omega t}$ terms and including the T, twist parameter. This gives the following form of the TE resonant mode field equations suitable for finding solutions for large aspect ratio toroidal cavities:-

$$Er = -A_{mn}\frac{m}{e_0 r}\left(J_m(kr)\right)\left[-C_2\sin(m\theta+T\phi)+D_2\cos(m\theta+T\phi)\right]\left[E_2\cos(p\phi)+F_2\sin(p\phi)\right]$$
$$\left[G_2\cos(\omega t)+H_2\sin(\omega t)\right] \tag{B.33a}$$

$$E_\theta = +A_{mn}\frac{k}{e_0}\left(-J_{m+1}(kr)+\frac{mJ_m(kr)}{kr}\right)\left[C_2\cos(m\theta+T\phi)+D_2\sin(m\theta+T\phi)\right]$$
$$\left[E_2\cos(p\phi)+F_2\sin(p\phi)\right]\left[G_2\cos(\omega t)+H_2\sin(\omega t)\right] \tag{B.33b}$$

$$E_\phi = 0 \tag{B.33c}$$

$$Hr = -A_{mn}\frac{k\beta}{\omega\mu_0 e_0}\left(-J_{m+1}(kr)+\frac{mJ_m(kr)}{kr}\right)\left[C_2\cos(m\theta+T\phi)+D_2\sin(m\theta+T\phi)\right]$$
$$\left[E_2\cos(p\phi)+F_2\sin(p\phi)\right]\left[G_2\cos(\omega t)+H_2\sin(\omega t)\right] \tag{B.33d}$$

$$H_\theta = -A_{mn}\frac{m\beta}{\omega\mu_0 e_0 r}\Big(J_m\left(kr\right)\Big)\Big[-C_2\sin\left(m\theta+T\phi\right)+D_2\cos\left(m\theta+T\phi\right)\Big]$$

$$\Big[E_2\cos\left(p\phi\right)+F_2\sin\left(p\phi\right)\Big]\Big[G_2\cos\left(\omega t\right)+H_2\sin\left(\omega t\right)\Big] \tag{B.33e}$$

$$H_\phi = -A_{mn}\frac{k^2}{\omega\mu_0 e_0}\Big(J_m\left(kr\right)\Big)\Big[C_2\cos\left(m\theta+T\phi\right)+D_2\sin\left(m\theta+T\phi\right)\Big]$$

$$\Big[E_2\sin\left(p\phi\right)-F_2\cos\left(p\phi\right)\Big]\Big[G_2\cos\left(\omega t\right)+H_2\sin\left(\omega t\right)\Big] \tag{B.33f}$$

Note: In the above equations the values of the parameters and constants can be obtained as follows:-
1) Those parameters required to produce some typical TE_{mnp} modes are:-
  a) For a normal full wave resonant TE_{111} mode with no twist:-

$$m=1,\ \ n=1,\ \ p=1\ \ \text{and } T=0 \tag{B.34}$$

  b) For a circularly polarised one wavelength mode:-

$$m=1,\ \ n=1,\ \ p=0\ \ \text{and } T=-1 \tag{B.35}$$

  c) The field which has usually been modelled in this paper is a half wave resonant $TE_{11\frac{1}{2}}$ mode with 180 degree clockwise twist which has:-

$$m=1,\ \ n=1,\ \ p=\frac{1}{2}\text{ and } T=-\frac{1}{2} \tag{B.36}$$

2) A positive value of T will give a field that twists in the $-\theta$ direction as ϕ increase i.e. twists anticlockwise with increasing ϕ angle. A negative T value field will twist clockwise as ϕ increases.

3) A_{mn}, e_0 and μ_0 are the same constants referred to in the notes for eqns (B.2).

4.1) The exact field form, such as whether it is stationary, rotating, the direction of rotation and the field orientation in the toroid is determined by the value given to the phase constants. Using the same values for both the E and H fields will give a toroidal travelling field moving in the $+\phi$ direction. Some examples of the effect of different phase constants for the half wave $TE_{11\frac{1}{2}}$ mode with T$=-\frac{1}{2}$ are described below.
a) For this first example, when $t=0$, the E field maximum will be at $\phi=0$ and be pointing towards $\theta=90$ degrees. The H field will be a minimum at $\phi=0$ and be pointing towards $\theta=180$ degrees :-

$$\text{E field: } C2=1, E2=1, G2=1 \qquad\qquad (D2=F2=H2=0) \tag{B.37}$$
$$\text{H field: } C2=1, E2=1, G2=1 \qquad\qquad (D2=F2=H2=0) \tag{B.38}$$

b) Starting with field 4.1.a above for both the E and H fields change E2 to 0 and F2 to +1 which will give both fields plus 90 degrees electrical (plus 180 degrees mechanical) phi rotation. Due to the theta rotation following the twist, the fields will also be rotated plus 90 degrees theta. The E field maximum will be at $\phi=180$ degrees and pointing towards $\theta=180$ degrees and the H field minimum at $\phi=180$ degrees and pointing towards $\theta=270$ degrees:-

$$\text{E field: } C2=1, F2=1, G2=1 \qquad\qquad (D2=E2=H2=0) \tag{B.39}$$
$$\text{H field: } C2=1, F2=1, G2=1 \qquad\qquad (D2=E2=H2=0) \tag{B.40}$$

c) Starting with field 4.1.b above in both the E and H field equations change C2 to $-C2$ for 180 degree theta rotation. This will give the electric field shown in Fig 3 and the magnetic field of Fig 5:-

$$\text{E field: } C2=-1, F2=1, G2=1 \qquad\qquad (D2=E2=H2=0) \tag{B.41}$$
$$\text{H field: } C2=-1, F2=1, G2=1 \qquad\qquad (D2=E2=H2=0) \tag{B.42}$$

d) All the above fields can be made to travel in the minus phi direction by rotating the magnetic field by 180 degrees theta which can be done by reversing the polarity of its second constant which will be E2 or F2 i.e. reverse the sign of whichever of these phase constants has a value of 1. For example using the field c) above change the value of the magnetic field F2 to -1:-

$$\text{E field: } C2=-1, F2=\ \ 1, G2=1 \qquad\qquad (D2=E2=H2=0) \tag{B.43}$$
$$\text{H field: } C2=-1, F2=-1, G2=1 \qquad\qquad (D2=E2=H2=0) \tag{B.44}$$

4.2) It is also possible to obtain a field poloidally spinning in the $\pm\theta$ direction by selecting different phase selection parameters for the E and H fields.

a) The anti-clockwise $(-\theta)$ spinning field in section 5 used the E field of Fig 3 and the H field of Fig 9. This moved with group velocity in the $+\phi$ direction and was obtained using the parameters:-

$$\text{E field: } C2 = -1, F2 = 1, G2 = 1 \qquad (D2 = E2 = H2 = 0) \qquad (B.45)$$

$$\text{H field: } D2 = 1, E2 = 1, G2 = 1 \qquad (C2 = F2 = H2 = 0) \qquad (B.46)$$

b) To have above field, 4.2.a, spinning in the $+\theta$ clockwise direction rotate just the magnetic field through 180 degrees theta by changing the sign of D2:-

$$\text{E field: } C2 = -1, F2 = 1, G2 = 1 \qquad (D2 = E2 = H2 = 0) \qquad (B.47)$$

$$\text{H field: } D2 = -1, E2 = 1, G2 = 1 \qquad (C2 = F2 = H2 = 0) \qquad (B.48)$$

c) To have above field, 4.2.b, moved so its initial E and H field maximums are at $\phi = 0$ instead of $\phi = 180$ degrees could be done by rotating the fields 180 degrees mechanical (90 degrees electrical) in the plus or minus phi direction. Each of these options will give different fields because as it is phi rotated the field will also theta rotate in the same direction as the twist. For $-\phi$ rotation the E field will point towards $\theta = 270$ degrees when it reaches $\phi = 0$ whereas for $+\phi$ rotation it will point towards $\theta = 90$ degrees. Similarly if the H field is $-\phi$ rotated, when it reaches $\phi = 0$ degrees it will point towards $+\phi$ from $\theta = 0$ to 180 degrees and towards $-\phi$ from $\theta = 180$ to 360 degrees, whereas for $+\phi$ rotation its direction will be reversed and point towards $-\phi$ from $\theta = 0$ to 180 degrees and towards $+\phi$ from $\theta = 180$ to 360 degrees. The fields will all still spin in the $+\theta$, clockwise, direction and because spin and twist are in the same direction the group velocity movement will be in the $-\phi$ direction

For $-\phi$ rotation use:-

$$\text{E field: } C2 = -1, E2 = 1, G2 = 1 \qquad (D2 = F2 = H2 = 0) \qquad (B.49)$$

$$\text{H field: } D2 = -1, F2 = -1, G2 = 1 \qquad (C2 = E2 = H2 = 0) \qquad (B.50)$$

For $+\phi$ rotation use:-

$$\text{E field: } C2 = -1, E2 = -1, G2 = 1 \qquad (D2 = F2 = H2 = 0) \qquad (B.51)$$

$$\text{H field: } D2 = -1, F2 = 1, G2 = 1 \qquad (C2 = E2 = H2 = 0) \qquad (B.52)$$

The difference between the two sets of fields above, which are produced by either + or - ϕ direction rotation of field 4.2.b, is just that the final theta angle is different. Specifically the $-\phi$ rotated field (B.49)/(B.50) is at +180 degrees theta relative to the $+\phi$ rotated field (B.51)/(B.52). It is therefore possible to produce the above $-\phi$ rotation field by turning the $+\phi$ rotation field through 180 degrees theta and this can be done by changing just the sign of the C2 and D2 phase selection constants as follows.

To produce the $-\phi$ rotation field from the $+\phi$ rotation (B.51) and (B.52) fields, change parameters to:-

$$\text{E field: } C2 = 1, E2 = -1, G2 = 1 \qquad (D2 = F2 = H2 = 0) \qquad (B.53)$$

$$\text{H field: } D2 = 1, F2 = 1, G2 = 1 \qquad (C2 = E2 = H2 = 0) \qquad (B.54)$$

To produce the $+\phi$ rotation field from the $-\phi$ rotation (B.49) and (B.50) fields, change parameters to:-

$$\text{E field: } C2 = 1, E2 = 1, G2 = 1 \qquad (D2 = F2 = H2 = 0) \qquad (B.55)$$

$$\text{H field: } D2 = 1, F2 = -1, G2 = 1 \qquad (C2 = E2 = H2 = 0) \qquad (B.56)$$

It interesting to note that the two sets of $-\phi$ rotation field phase selection constants (B.49)/(B.50) and (B.53)/(B.54) have different signs although the fields they produce are identical. The same applies with the two $+\phi$ rotation fields.

B.4.3 To Find the Remaining Unknowns for the Toroidal Cavity Field Equations

Equations have previously been given for finding k and β but for convenience they are repeated here:-

Eqn (B.13) gives the value of k for the TE_{11p} mode. This is only applicable when $n = 1$:-

$$k = \left(\frac{1.8412}{r_0} \right)$$

Eqn (B.21) for β:-

$$\beta = \left(\frac{p}{R} \right)$$

22

B.4.3.1 To Find The Resonant Frequency When R and r_0 Are Known. With the notes to eqns (B.33) and the above formulae all the toroidal field equation unknowns can be found once ω, R and r_0 are assigned values. The relationship between them can be obtained from eqn (B.24) which was for the toroid resonant frequency:-

$$f_e = \frac{c}{2\pi} \sqrt{\left(\frac{p}{R}\right)^2 + k^2}$$

Substituting in the above equation for k using eqn (B.13) results in the required relationship to enable the resonant frequency of a toroid of known size and containing p wavelengths to be obtained:-

$$f_e = \frac{c}{2\pi} \sqrt{\left(\frac{p}{R}\right)^2 + \left(\frac{1.8412}{r_0}\right)^2} \tag{B.57}$$

The ω used in the (B.33) field equations is just $2\pi f_e$.

B.4.3.2 To Find r_0 When the Resonant Frequency and Aspect Ratio Are Known. Alternatively, if the resonant frequency and the required toroid aspect ratio (AR=R/r_0) are known instead, then putting R equal to (AR r_0) in eqn (B.57) and solving for r_0 results in the following solution:-

$$r_0 = \frac{c}{2\pi f_e} \sqrt{\left(\frac{p^2}{(AR)^2} + 1.8412^2\right)} \tag{B.58}$$

Having found r_0 and knowing the aspect ratio enables R to be found and hence all the parameters for the field equations are again known.

B.4.3.3 To Find r_0 When the Resonant Frequency and R Are Known. Solving eqn (B.57) for r_0 gives the required formula directly:-

$$r_0 = \frac{1.8412}{\sqrt{\left(\frac{2\pi f_e}{c}\right)^2 - \left(\frac{p}{R}\right)^2}} \tag{B.59}$$

B.4.3.4 To Find the Required Toroid Size For a Desired Resonant Frequency and Phase Velocity. It is often useful to have a toroid with a known phase velocity The additional equations needed to do this are:-
Eqn (B.12) :-

$$v_p = \frac{\omega}{\beta c}$$

Eqn (B.16):-

$$\beta = \sqrt{\frac{\omega_e^2}{c^2} - k^2}$$

Squaring eqn (B.16) and dividing the result by β^2 gives:-

$$1 = \frac{\omega_e^2}{c^2 \beta^2} - \frac{k^2}{\beta^2} \tag{B.60}$$

Use eqn (B.12) to substitute v_p^2 for $\frac{\omega_e^2}{c^2\beta^2}$, eqn (B.13) to substitute for k^2 and eqn (B.21) to substitute for β^2 in the last term:-

$$1 = v_p^2 - \frac{1.8412^2 R^2}{r_0^2 p^2} \tag{B.61}$$

R/r_0 is the toroid aspect ratio (AR), so solving eqn (B.61) for this results in the required relationship:-

$$AR = \frac{p}{1.8412} \sqrt{v_p^2 - 1} \tag{B.62}$$

The toroid aspect ratio and resonant frequency are now known and once again eqn (B.58) can be used to give the complete solution of all the unknowns.

APPENDIX C

C   - Some Techniques For Measuring Toroidal Field Parameters

Time animations of 3D plots of the electric and magnetic fields are usually the most useful way to get an overall view of the form of the toroidal cavity field and how it is changing with time. This is particularly important when needing to identify if say toroidal or poloidal rotation of a twisted field is occurring and in this case consideration of the direction of the Poynting vector is also very helpful. However, a 3D plot often does not show the field precisely enough to take accurate measurements and if only a small change to the field occurs this may not even be visible. There are a large number of alternative plots which could be taken but the one which has frequently been used here is of the magnitude of each individual vector field component, particularly those of the electric field, plotted against the phi toroidal angle. It is not intended to cover all the many different possibilities but instead to give more information on how the toroidal field measurements quoted have been obtained. The description refers specifically to the results for the toroidally spinning $TE_{11\frac{1}{2}}$ field of section 4 in the main document but the general method can also be applied to other modes.

C.1   Field Measurement Reference Points

To determine the movement of the field structure more accurately over time a plot of the magnitude of the individual field components against phi angle has certain features which can be used to establish reference points. If further plots are taken at consecutive time steps it becomes obvious that some of the field zero points are moving rapidly in the phi direction over just a few time steps whilst others appear stationary but move slowly over a longer time period. Fast movement is likely to be associated with phase velocity movement and slow movement with group velocity. For a perfect theoretical TE_{11} field, assuming the measuring point is at $\theta = $ x degrees and r is not at the toroid wall or at r equals zero then typical reference points could be:-

Ref 1) If, at the measuring point theta angle, both E_r and E_θ are zero at some phi angle then both these electric fields are zero magnitude across the complete toroid minor cross section at this phi location.

Ref 2) If just E_θ is zero at a particular phi angle the electric field is aligned pointing along the theta equals x+0 to x+180 degree minor diameter.

Ref 3) If just E_r is zero at a particular phi angle the electric field is aligned pointing along the theta equals x+90 to x+270 degree minor diameter.

In Fig 8 of the main document the electric field measuring position is at $\theta = 0$ degrees so x is zero. Reference points 1 at $\phi = 0$ degrees and 2 at $\phi = 180$ degrees are visible and these numbers are marked on that figure. A similar plot, Fig C.1, taken at t=14 time steps, which is after just over $\frac{1}{8}$th of a cycle electrical or $\frac{1}{4}$ of a revolution, after the start of the FDTD program, shows that in fact all three reference points are present. Point 1 which was previously combined with point 3 has now moved at phase velocity to just beyond the $\phi = 90$ degree position, revealing both points. Looking at the 3D electric field plot Fig 7, which is also at time step 14, confirms the validity of the reference point 2 and 3 field alignments and the movement of the zero field magnitude reference point 1. Alignment along axes at different theta angles can be found using reference points 2 and 3 by changing the value of the theta angle measuring point, x. Additional reference points may also be found if the magnetic field is plotted instead.
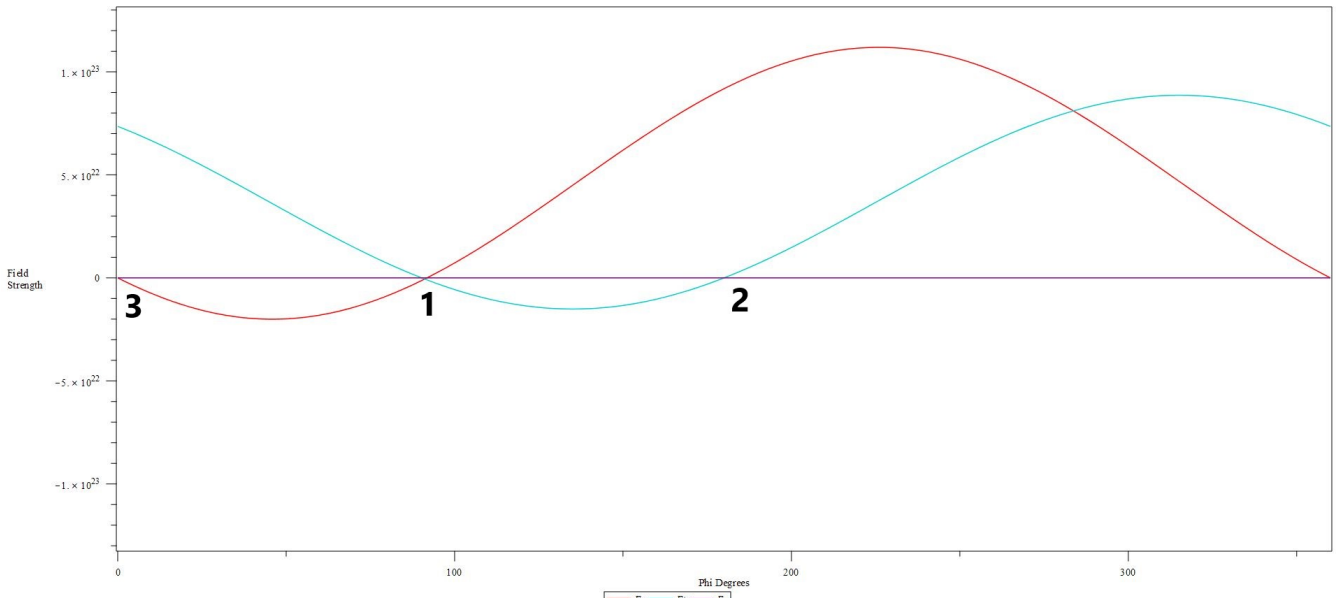
Figure C.1: Amplitude Variation of E_r and E_θ Electric Field Components With ϕ Angle.
Shown After Just Over $\frac{1}{8}$th Of a Cycle.

C.2   Example of Reference Point Measurements of Section 4 Toroidally Spinning Field at Phi $\approx$ 189 Degrees.

It is useful to plot the fields not only at $\theta = x$ but also at the diametrically opposite position $\theta = x + 180$ degrees. A typical plot is shown in Fig C.2. Considering first the E_θ field, which is the turquoise blue lines, it can be seen that this is an alternative plot of Fig 8b taken over a very small phi angle range and shows with much greater accuracy the amount of movement of the phi equals 180 degree reference point 2. The measuring points are now at $r = 2$ and the $\theta = 0$ and 180 degree positions. Both pass through zero at the same phi angle with remarkably and somewhat unexpectedly good agreement.

Some readers will be aware that in FDTD programs the field calculation positions are not at the points where the grid lines intersect but half way along the grid squares. This needs to be taken into account when plotting or calculating field values and if not considerable errors would be introduced in the high resolution phi direction plots being used. To prevent this all plots in this paper use field values which have been calculated at the grid line intersection positions using linear interpolation between the half grid square locations. This can introduce interpolation errors but generally these will be small.
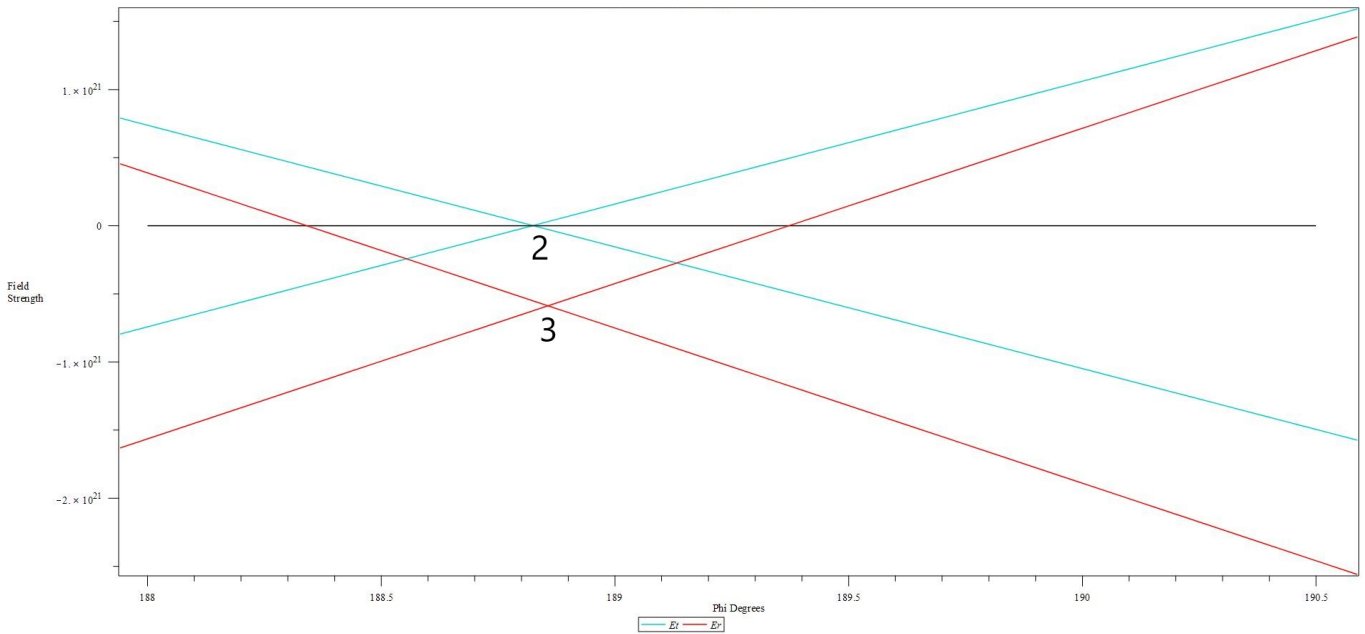
Figure C.2: High Resolution Plot of E_θ and E_r Field Zero Magnitude Positions For t=99996.
(Turquoise E_θ Rising Line at $\theta = 0$ degrees, Falling Line at $\theta = 180$ degrees)
(Red E_r Rising Line at $\theta = 90$ degrees, Falling Line at $\theta = 270$ degrees)

25

A different potential difficulty still arises with this measurement though because the use of twist is likely to result in a mode with toroidal rotation also producing poloidal rotation and vice versa, as shown in section 6 of the main paper. Any poloidal movement can cause the reference point field zero to no longer be at a fixed phi angle over the short term but instead the phi angle changes slightly over a single cycle. To check for this it is easiest to produce a time animation of Fig C.2, the reference position plot. Although a time animation can not be shown in this paper looking at Fig 8a it can be seen that the 'hidden' reference point 3, E_r field, is at a tangent to the phi angle axis. This situation normally occurs whenever reference point 1 is at the same phi angle as reference points 2 or 3 and is very easily identified in a time animation and the time steps at which this takes place can be found very accurately. The number of time steps between consecutive tangent events at one particular reference point will be exactly half a cycle, corresponding to one mechanical field revolution. Using the time step midway between these events to find the phi angle for the mean position of the reference point largely eliminates errors due to short timescale poloidal movements. Fig C.2 was actually obtained in this way and and taken at the midway time step, which was found to be number 99996. This plot shows a travel of 8.82 phi degrees which compares with a calculated value of 8.89 degrees using eqn (3) and is a -0.79% difference. The potential poloidal rotation likely with this mode and the effect it has of moving the E_θ and E_r field line intersection points in the plus or minus phi directions in a time animation means that this can also be used to detect small levels of theta direction rotation.

The red lines in Fig C.2 are similar plots of the E_r field. This is a reference point 3 plot but with the measuring points at theta equals 90 and 270 degrees, which is using an x value of 90 degrees and is an alternative way of finding when the E field is aligned along the 0 to 180 degree axis. Interestingly the two measuring point lines no longer cross the zero field value at the same phi angle. Calculating the phi angle value at a position midway between the two zero field phi angle positions gives the mean value for the phi angle travel of the field which in this case is 8.84 degrees. If the two E_r lines had the same slope the mean value would be where the two lines cross which is nearly the case as the crossing point is at a travel of 8.86 phi degrees. The 8.84 degree travel is an error of -0.56% compared with eqn (3). and this and the above result for E_θ confirm that the long term toroidal rotation of the field is at the group velocity.

The reason for the two E_r field lines not crossing zero at the same phi angle was found to be because the centre of the E field is slightly offset from the centre of the minor diameter. It is known that in toroids the field centre can move inward or outward along the direction of the major radius although there is not always agreement in the literature on which direction is correct. Compare for example Kark [11] (outward) and Keil [12] (inward). Where the two E_r lines cross at point 3 in the figure the field values at $\theta = 90$ and 270 degrees are the same so this is the phi angle at which the main electric field direction is parallel to the 0 to 180 degree line. To find out the direction and magnitude of the field offset it is necessary to interpolate between the actual FDTD calculated field values, including allowing for these values often being found half a grid square away from the grid intersection in an FDTD program. Details of this calculation are not shown but the offset was found to be inward along the major radius but of a very small distance of just 1.5% of the theta length of a grid square positioned at $r = 2$. It is reference points measured along the theta=90 to 270 degree line which should be most affected and one along the theta=0 to 180 degrees line should show no offset due to this cause, which is what is shown for the E_θ field line crossing point in Fig C.2.

C.3 Example of Reference Point Measurements of Section 4 Toroidally Spinning Field at Phi ≈ 9 Degrees.

A similar plot can be made of the E_r field, which at the start of the simulation is at phi equals zero degrees. In this case, as Fig 8b shows because the E_r field approaches zero at a tangent the exact zero crossing position is hard to measure accurately. Using the above technique, though, it is the time midway between two time steps which have the field tangent to the zero line which should be used instead. In this case the exact E_r tangent was found to occur at 99994 (not 99996) and 100048 giving the midway position time step as 100021. This is approximately one quarter of a cycle (electrical) later where the zero crossing is steep and easily measured. The additional time steps when calculating movement at t=100021 instead of 99996 will slightly increase the theoretical calculated movement but to two decimal places should still be 8.89 degrees. As shown in Fig C.3 the measured movement in this case is 8.97 degrees which is an error of +0.90%.

The E_θ field can also be plotted around the phi=9 degrees position but because the 3D field is aligned pointing along along the 90 to 270 degree axis, x needs to be 90 degrees giving theta angles of 90 and 270 degrees for the measurement instead of 0 and 180 degrees as was used for the E_r measurement. It can be seen that it is the E_θ field crossing, which no longer takes place at zero field angle, and as this is being measured along the 90 to 270 degree line it supports the theory that it is the main field being offset along the major radius which is responsible for having field component lines not crossing each other at zero field magnitude.

The discrepancy between the group velocity measurements at the approximately 9 and 189 phi degree locations seems to be due to very slight poloidal movement of the field starting to occur however the agreement is good enough to confirm that the field is moving toroidally at the group velocity.
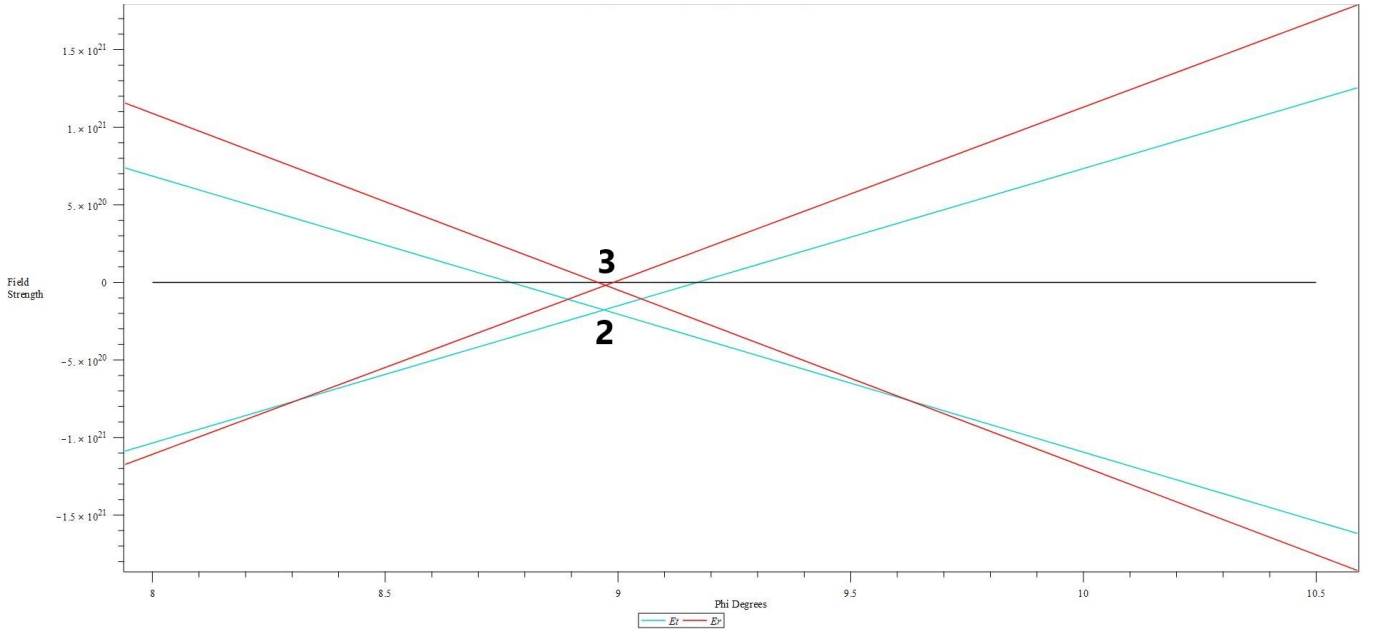
Figure C.3: High Resolution Plot of E_θ and E_r Field Zero Magnitude Positions For t=100021.
(Turquoise E_θ Rising Line at $\theta = 90$ degrees, Falling Line at $\theta = 270$ degrees)
(Red E_r Rising Line at $\theta = 180$ degrees, Falling Line at $\theta = 0$ degrees)

C.4   Results of Investigating the Polarity of the Field Component Crossing and Direction of Main Field Offset

It was the need to find the reason for the field components not always crossing at zero field amplitude in the high resolution phi direction plots which led to investigating the offset of the main field inward or outward along the major radius. However, the offset is small and although an interesting effect it so far seems to be of limited importance and therefore has not been fully investigated. Whilst not wishing to excessively examine the matter it was thought worthwhile to give the results of the measurements actually taken and these are summarised in Table C1. They comprised four measurements and calculations which were taken over a complete electrical cycle, which was two mechanical revolutions of the field.

Table C1: Relation Between Field Component Crossing Polarity and Main Field Offset

Time Step Number	Field Component	Approx. Phi Angle (Deg)	Field Crossing Polarity	Main Field Points To θ Degrees	Offset Direction	Offset Amount
99967	E_θ	9	+ve	270	Inward	0.88%
100021	E_θ	9	-ve	90	Inward	0.47%
99996	E_r	189	-ve	0	Inward	1.5%
100048	E_r	189	-ve	180	Outward	2.1%

There are several things worth noting, for example, whether the offset is inwards or outwards is not determined just by looking at the sign of the electric field at the crossing point in the high resolution plots. This is because the field sign at the crossing point is also effected by the sign of the main electric field and that is dependant upon the direction in which the total electric field points. This relationship is also different for E_r and E_θ fields.

A more surprising feature is that the direction of the main field offset varies and although it is normally inwards, at time step 100048 when the main field points outwards, the offset at the θ=180 degrees was found to change and become outwards. To confirm this further checks would be necessary such as checking the accuracy of the FDTD calculation by using a finer FDTD grid with more grid squares and seeing if this changed the result. It would also be interesting to check the measurement for the simpler case of the basic stationary field with say radial and then z axis polarisation directions and also using toroids with different aspect ratios. It seems to be a more complicated issue requiring more investigation than might first be assumed.

References

[1] F. Cap and R. Deutsch, "Toroidal resonators for electromagnetic waves," *IEEE Transactions on Microwave Theory and Techniques*, vol. 26, no. 7, pp. 478–486, 1978.

[2] R. Deutsch, "Toroidal resonator with a conducting separating wall," *IEEE Transactions on Microwave Theory and Techniques*, vol. 27, no. 2, pp. 172–178, 1979.

[3] R. Deutsch, "The influence of the energy dissipation and of the geometry on toroidal resonators with a conducting separating wall," *IEEE Transactions on Microwave Theory and Techniques*, vol. 28, no. 9, pp. 1014–1017, 1980.

[4] C. A. Balanis, *Advanced engineering electromagnetics*. John Wiley & Sons, 2012.

[5] M. Glen, "Spinning electromagnetic fields," *Web site previously https://mike2017.000webhostapp.com, now at www.spinningelectromagneticfields.com*, First published 2005.

[6] L. Allen, M. W. Beijersbergen, R. Spreeuw, and J. Woerdman, "Orbital angular momentum of light and the transformation of laguerre-gaussian laser modes," *Physical review A*, vol. 45, no. 11, p. 8185, 1992.

[7] L. Allen, S. M. Barnett, and M. J. Padgett, *Optical angular momentum*. CRC press, 2003.

[8] D. Hestenes, "The zitterbewegung interpretation of quantum mechanics," *Foundations of Physics*, vol. 20, no. 10, pp. 1213–1232, 1990.

[9] D. Hestenes, "Zitterbewegung structure in electrons and photons," *arXiv preprint arXiv:1910.11085*, 2019.

[10] H. R. L. Lamont, *Wave guides*. Methuen, 1942.

[11] K. W. Kark, "Perturbation analysis of electromagnetic eigenmodes in toroidal waveguides," *IEEE transactions on microwave theory and techniques*, vol. 39, pp. 631–637, Apr. 1991.

[12] R. Keil, "Numerical calculation of electromagnetic toroidal resonators," *Archiv Elektronik und Uebertragungstechnik*, vol. 38, pp. 30–36, 1984.